Accelerative oxygen evolution by Cu-doping into Fe-Co oxides

Qiaoqiao Zhang,[#] Ning Liu,[#] Jingqi Guan*

Key Laboratory of Surface and Interface Chemistry of Jilin Province, College of Chemistry, Jilin University, Changchun 130021, PR China.

*E-mail: guanjq@jlu.edu.cn (J. Guan)

[#]These authors contributed equally to this work.

Experimental section

Synthesis of $FeCoCuO_x$

$FeCoCuO_x$ oxide was prepared by a modified sol-gel method.[1] Typically, 0.162 g (1.0 mmol) of ferric trichloride, 0.13 g (1.0 mmol) of cobalt chloride and 0.134 g (1.0 mmol) of cupric chloride were dissolved in 2 mL ethanol, which were denoted as solution A. 0.1 mL of deionized water was dissolved in 2 mL of ethanol, which were nominated as solution B. After the solution A and solution B were cooled down to zero degree, the solution B was added to solution A to form a pellucid solution. Then, 1 mL of precooled propylene oxide was dropwise added to the above mixture under vigorous stirring. The obtained gel was aged for 24 h and then extracted with acetone for five times. The solid was dried by freeze drying method to obtain sandybrown $FeCoCuO_x$.

For comparison, FeO_x, CoO_x, CuO_x, $FeCuO_x$, $FeCoO_x$, and $CoCuO_x$ were synthesized following a process similar to that for $FeCoCuO_x$.

Characterization

Transmission electron microscope (TEM) images were observed by a HITACHI HT7700. High-resolution TEM (HRTEM) images were recorded on a JEM-2100 transmission electron microscope (Tokyo, Japan) at 200 kV. SEM images were recorded on a HITACHI SU8020 field emission scanning electron microscope. The valence state was determined using XPS recorded on a Thermo ESCALAB 250Xi. The X-ray source selected was monochromatized Al Kα source (15 kV, 10.8 mA).

Region scans were collected using a 20 eV pass energy. Peak positions were calibrated relative to C 1s peak position at 284.6 eV. Inductively coupled plasma atomic emission spectrometer (ICP-AES) was performed on a Shimadzu ICPS-8100.

Electrochemical measurements

All electrochemical measurements were performed on an electrochemical working station at room temperature. The catalysts were measured in 1.0 M KOH aqueous solution using a typical three-electrode configuration, in which glassy carbon electrode (platinum electrode or nickel foam) was used as the working electrode; platinum plate and saturated calomel electrode (SCE, saturated KCl) were used as the counter and reference electrodes, respectively. All potentials reported here in this work were calibrated against the reversible hydrogen electrode (RHE) (Figure S2). The working electrode was first activated by steady-state cyclic voltammetry (CV) performed in the potential range from 1.0 to 1.5 V vs RHE at a scan rate of 50 mV s^{-1} for 50 cycles. Linear sweep voltammetry (LSV) polarization curves were acquired at a scan rate of 1 $mV \cdot s^{-1}$. Electrochemical impedance spectroscopy (EIS) measurements were performed at open-circuit potential in the frequency range from 100 kHz to 0.1 Hz with an a.c. perturbation of 5 mV.

One millilitre of homogeneous catalyst ink was obtained by sonication for 30 min, consisting of 4 mg of catalyst, 20 μL of Nafion solution (5%), and 980 μL of water. All the catalyst ink was dropped on the pre-polished glassy carbon electrode (~0.4 mg·cm^{-2}).

Calibration of SCE and conversion to RHE

The reference electrode SCE was calibrated according to the method reported previously.[2-4] Calibrations were carried out by using a reversible hydrogen electrode (RHE). First, two Pt electrodes were cleaned by cycling in 1 M H_2SO_4 between -2 and 2 V for 2 hours. Then, they were used as working electrode and counter electrode, respectively. Before the calibration, the 1.0 M KOH electrolyte should be saturated with H_2 by continuous bubbling H_2. During the calibration, hydrogen was bubbled over the working electrode. A series of controlled-potential chronoamperometric curves were measured for 300 s to get the current interconvert between the hydrogen oxidation and hydrogen evolution reaction. The resulting potential is the potential of zero net current. In this work, the potential of zero net current was found at -1.038 V versus the SCE electrode in 1.0 M KOH (Figure S2). Thus, the potentials, measured against SCE, were converted into the potentials versus RHE by using the equation 1:

$$E_{vs.RHE} = E_{vs.SCE} + 1.038\ V \qquad (1)$$

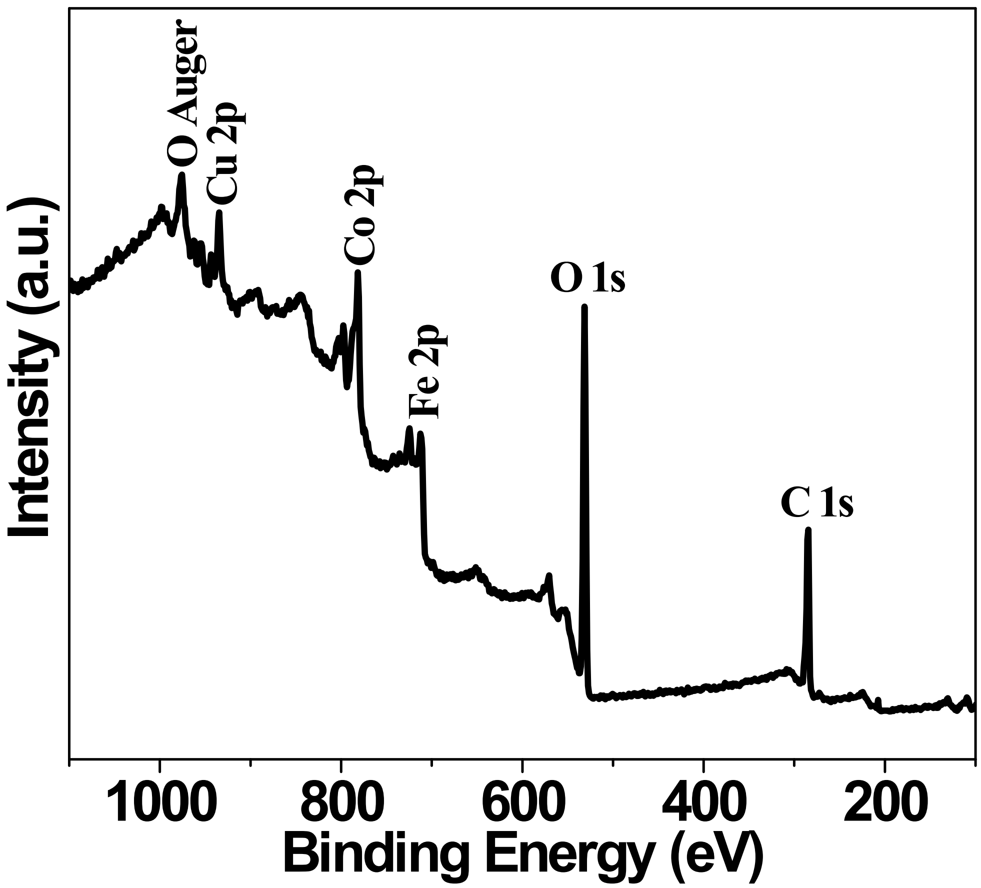

Figure S1. XPS survey spectrum of FeCoCuO$_x$.

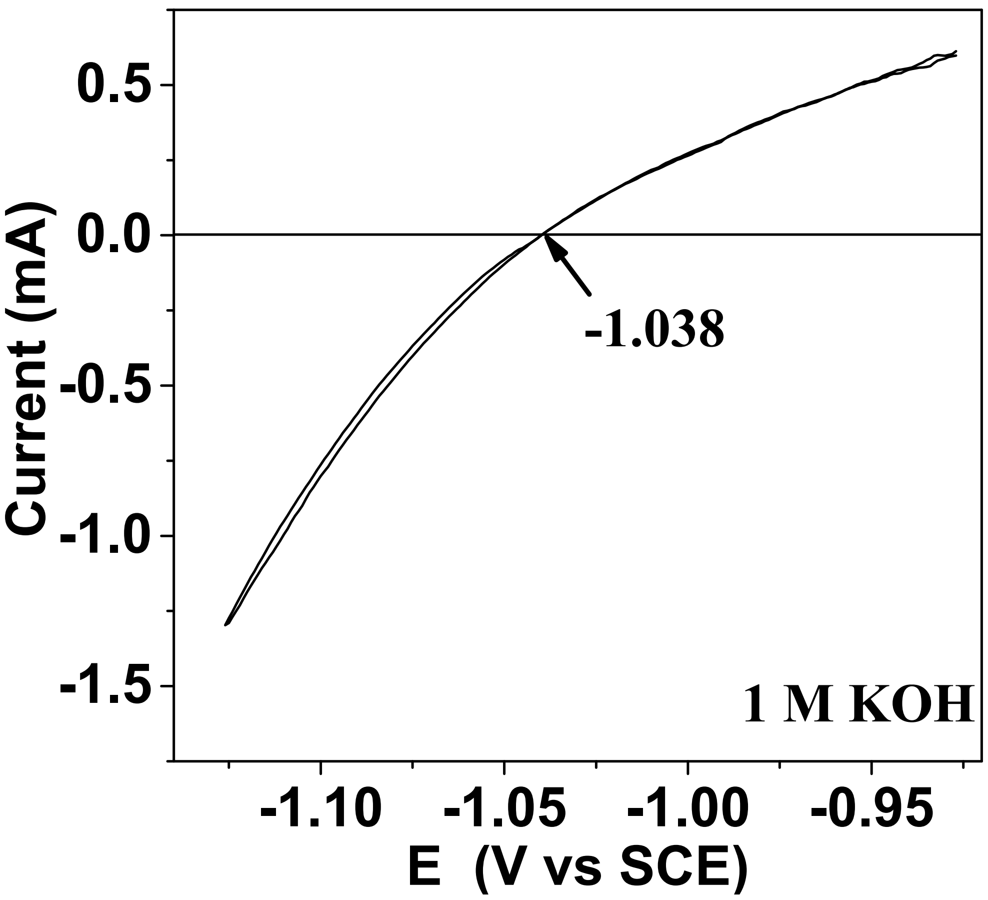

Figure S2. The current as a function of the applied potentials for the calibration of SCE reference electrode in 1.0 M KOH.

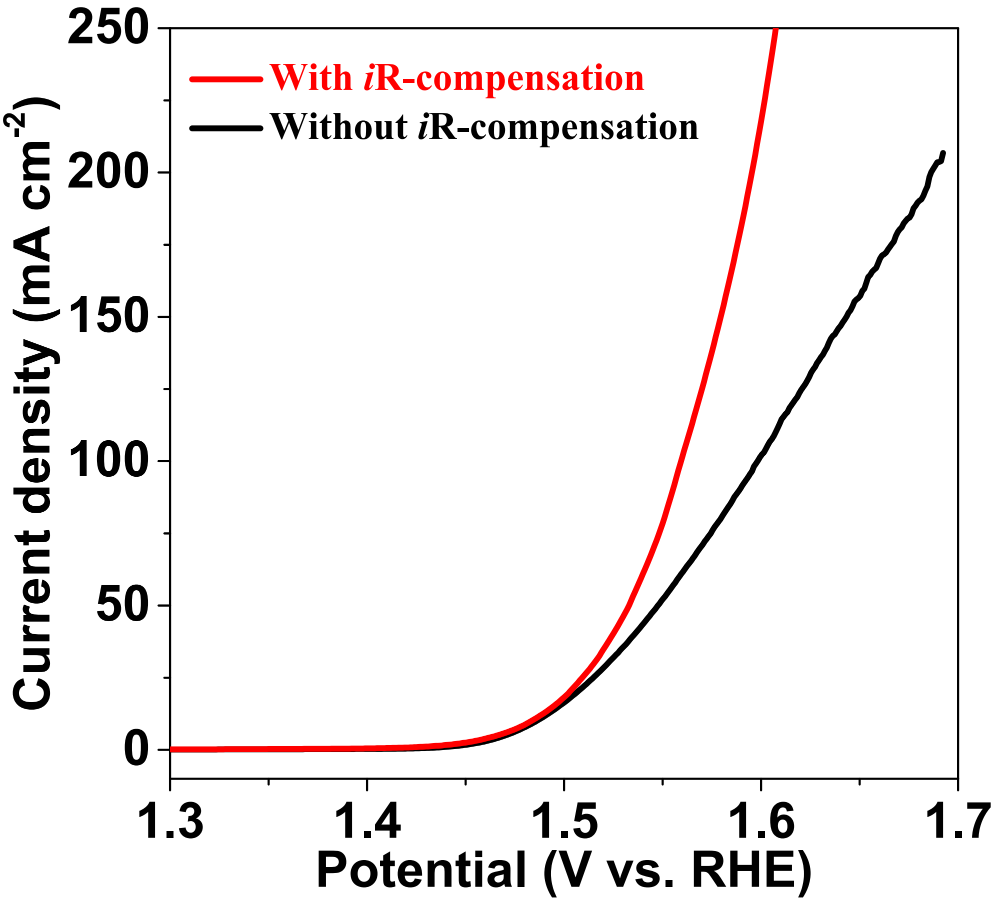

Figure S3. Polarization curves of FeCoCuO$_x$ supported on GCE in 1.0 M KOH solution with and without *iR*-compensation.

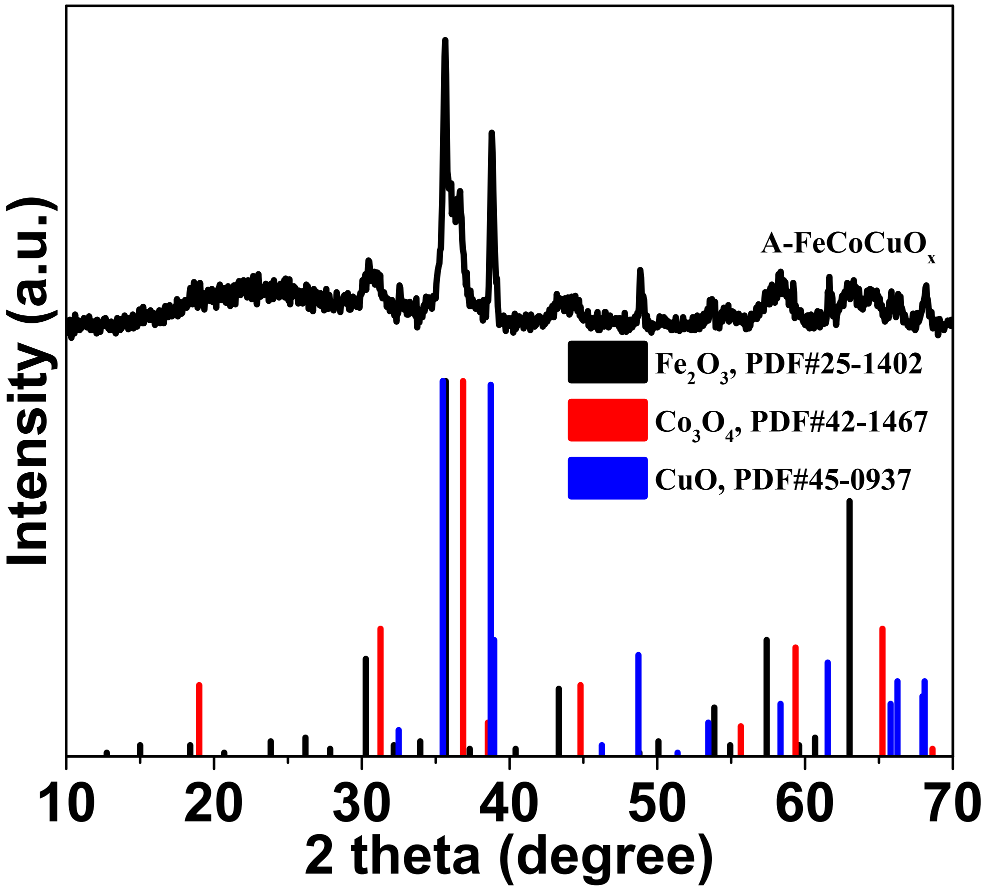

Figure S4. XRD patterns of A-FeCoCuO$_x$ and referred samples (Fe$_2$O$_3$, Co$_3$O$_4$, and CuO).

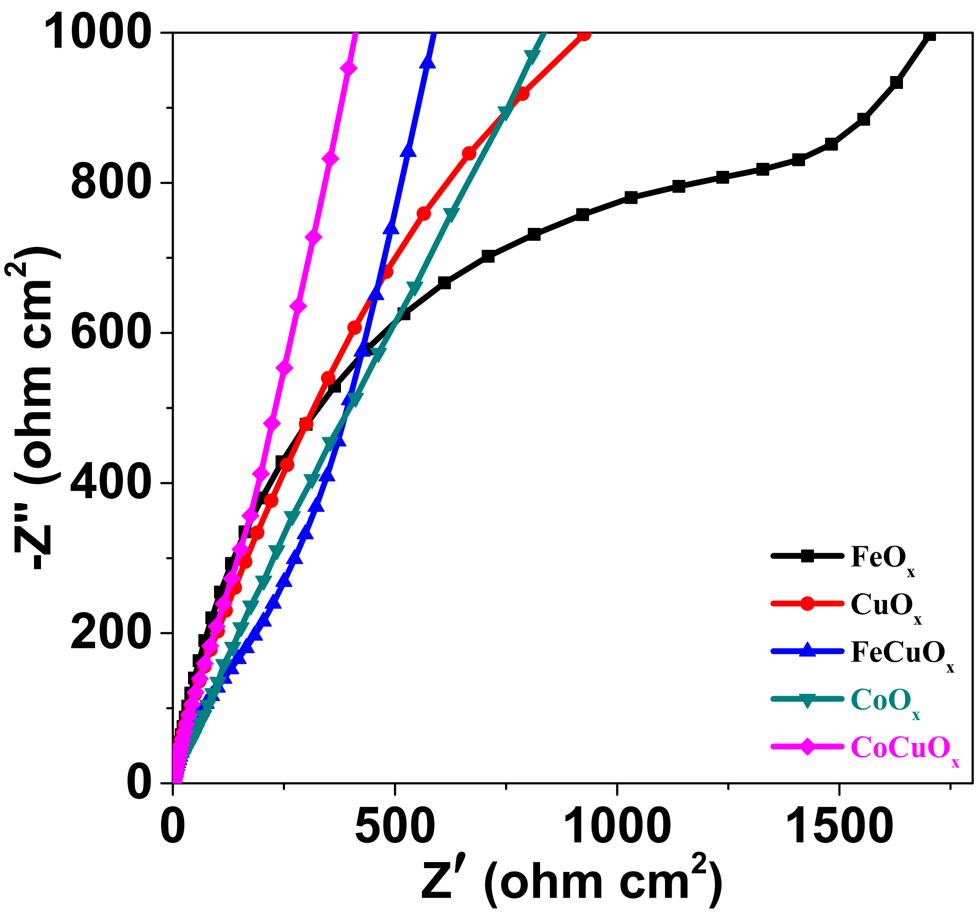

Figure S5. Nyquist plots of the EIS test for the FeO$_x$, CoO$_x$, CuO$_x$, FeCuO$_x$, and CoCuO$_x$.

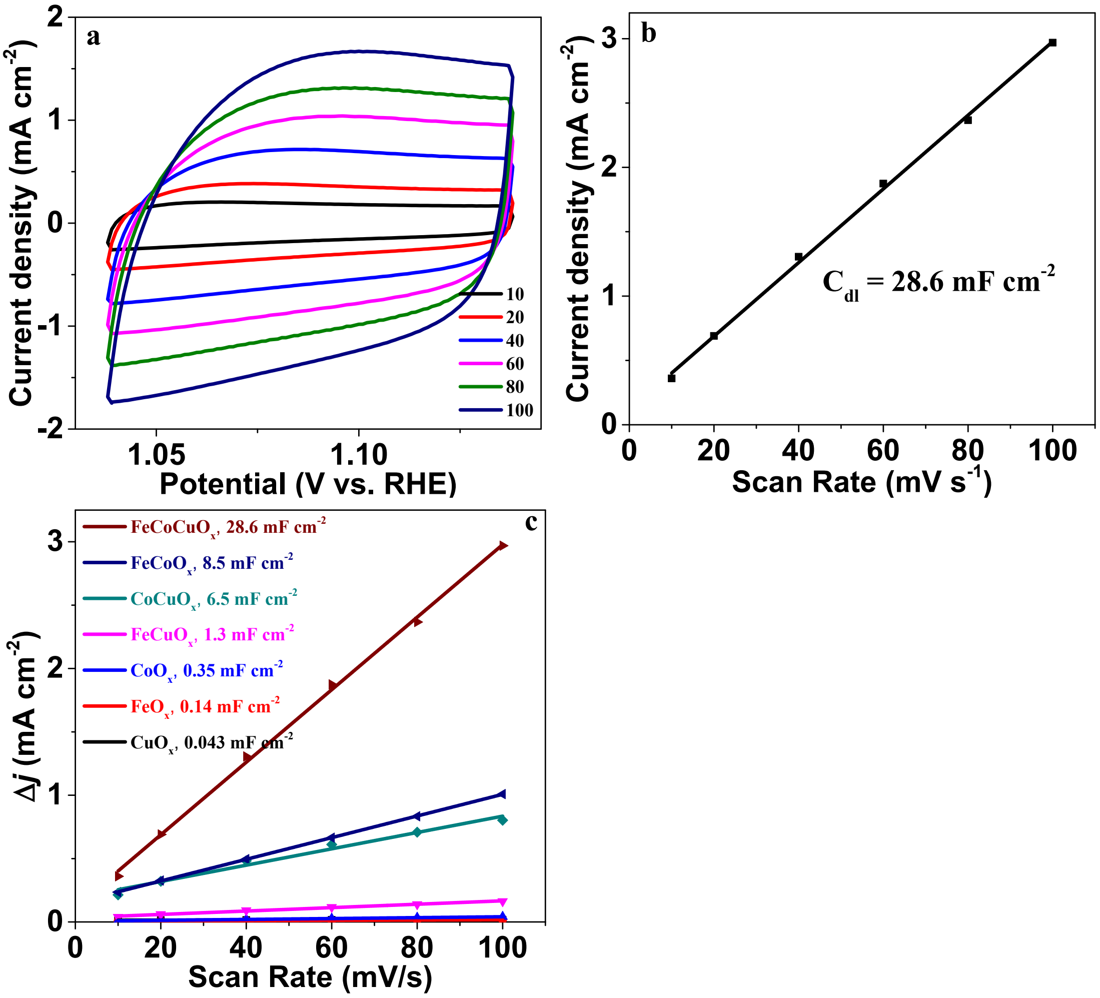

Figure S6. (a) CVs of FeCoCuO$_x$ measured in a non-Faradaic region (from 0 to 0.1 V vs. SCE) at scan rate of 10 mV s^{-1}, 20 mV s^{-1}, 40 mV s^{-1}, 60 mV s^{-1}, 80 mV s^{-1}, and 100 mV s^{-1}. (b) Capacitive *j* vs scan rate for FeCoCuO$_x$ anode. The linear slope is equivalent to twice of the double-layer capacitance C_{dl}. (c) Capacitive *j* vs scan rate for CuO$_x$, FeO$_x$, CoO$_x$, FeCuO$_x$, CoCuO$_x$, FeCoO$_x$, and FeCoCuO$_x$.

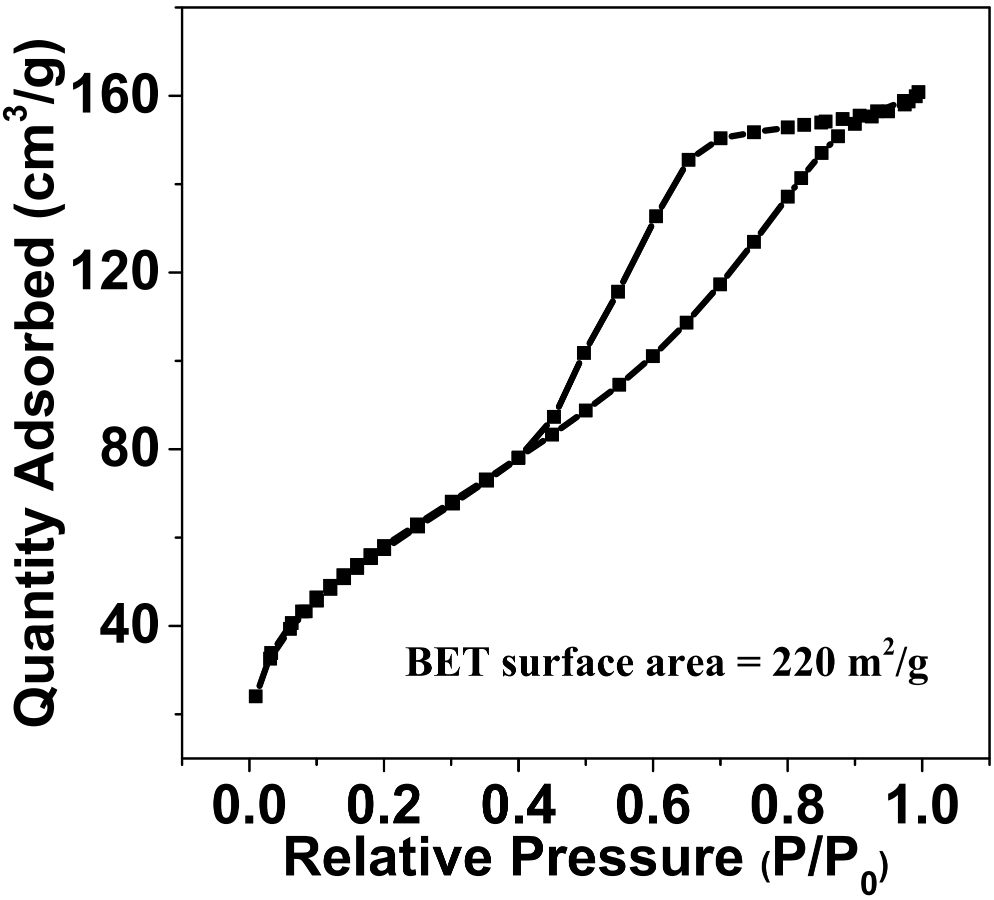

Figure S7. N_2 adsorption–desorption isotherms of $FeCoCuO_x$.

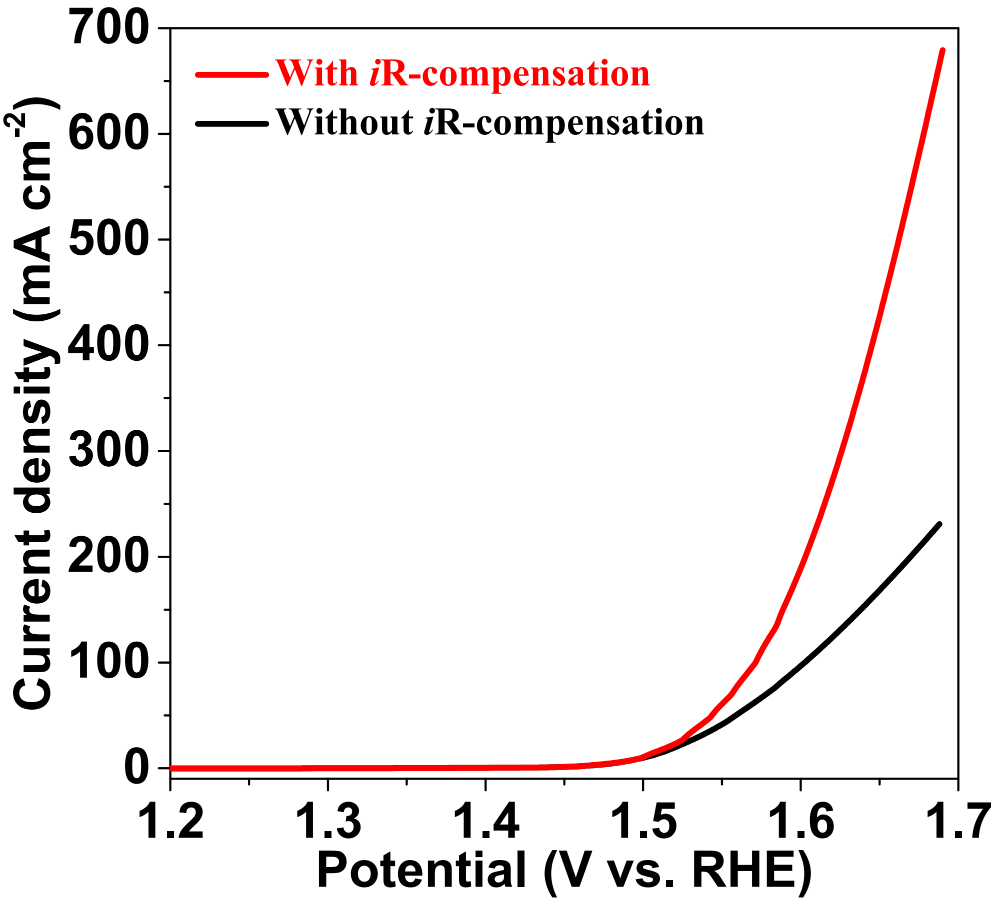

Figure S8. Polarization curves of $FeCoCuO_x$ supported on Pt electrode in 1.0 M KOH solution with and without *iR*-compensation.

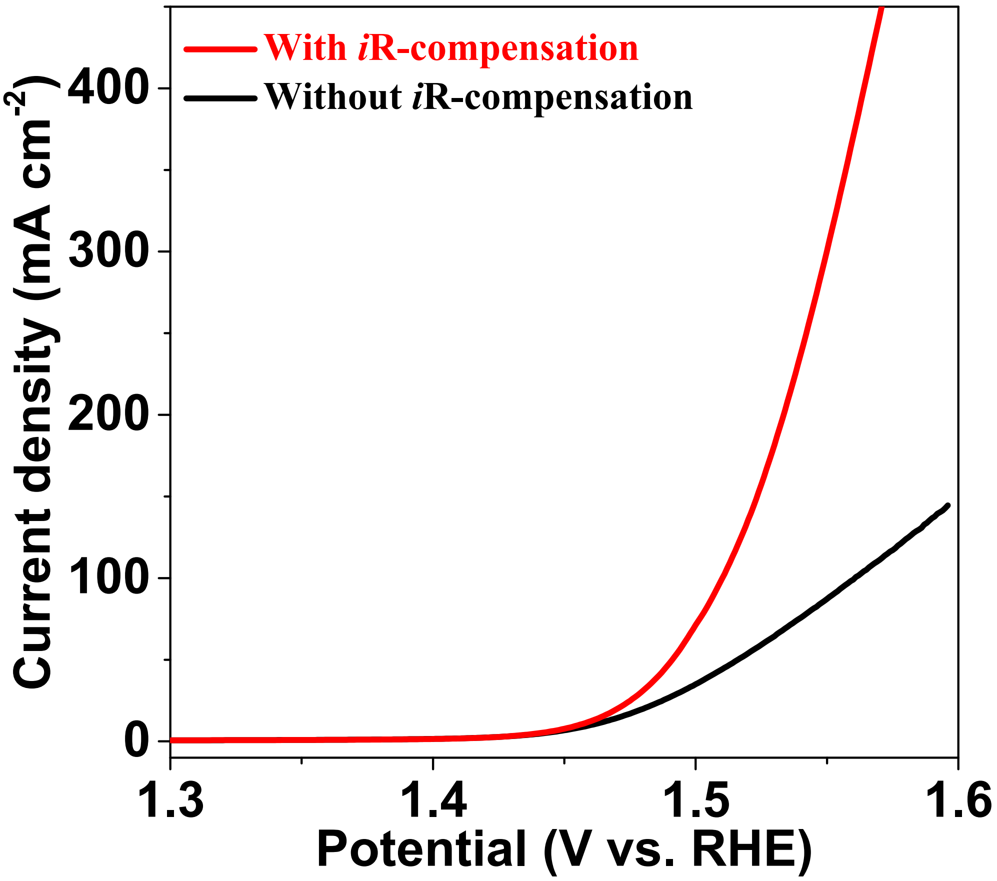

Figure S9. Polarization curves of $FeCoCuO_x$ supported on nickel foam electrode in 1.0 M KOH solution with and without *iR*-compensation.

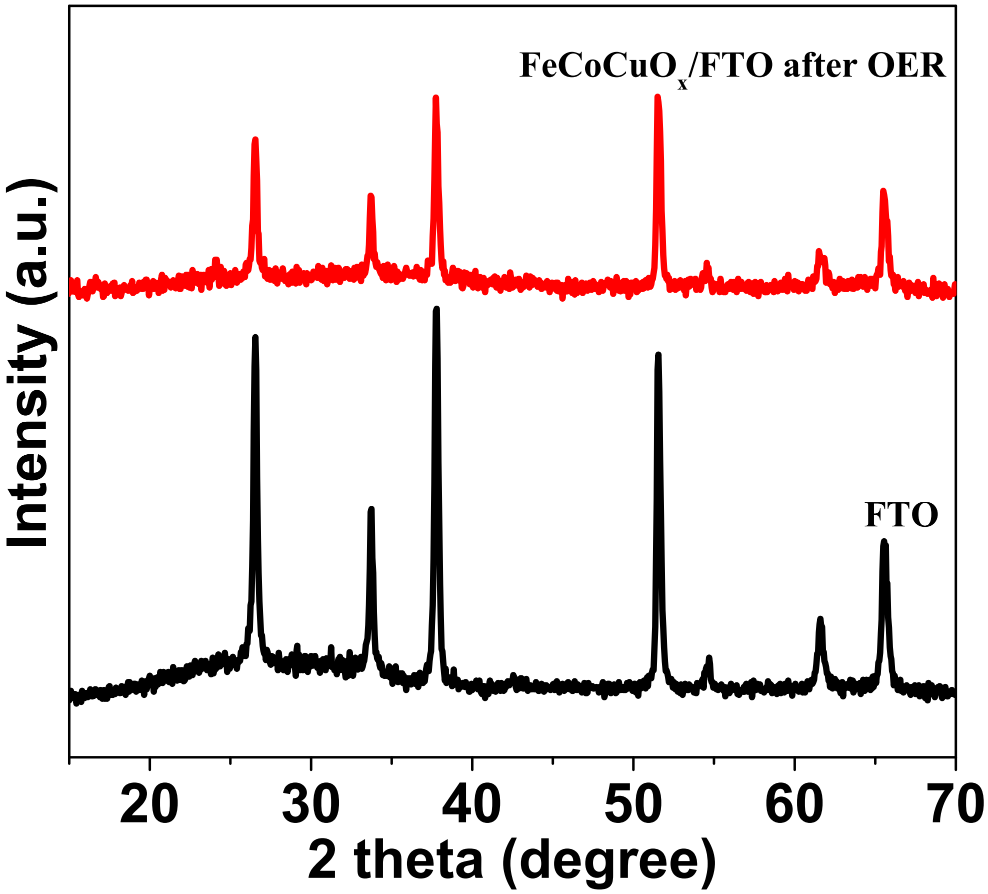

Figure S10. XRD patterns of FTO and FeCoCuO$_x$/FTO after OER stability test.

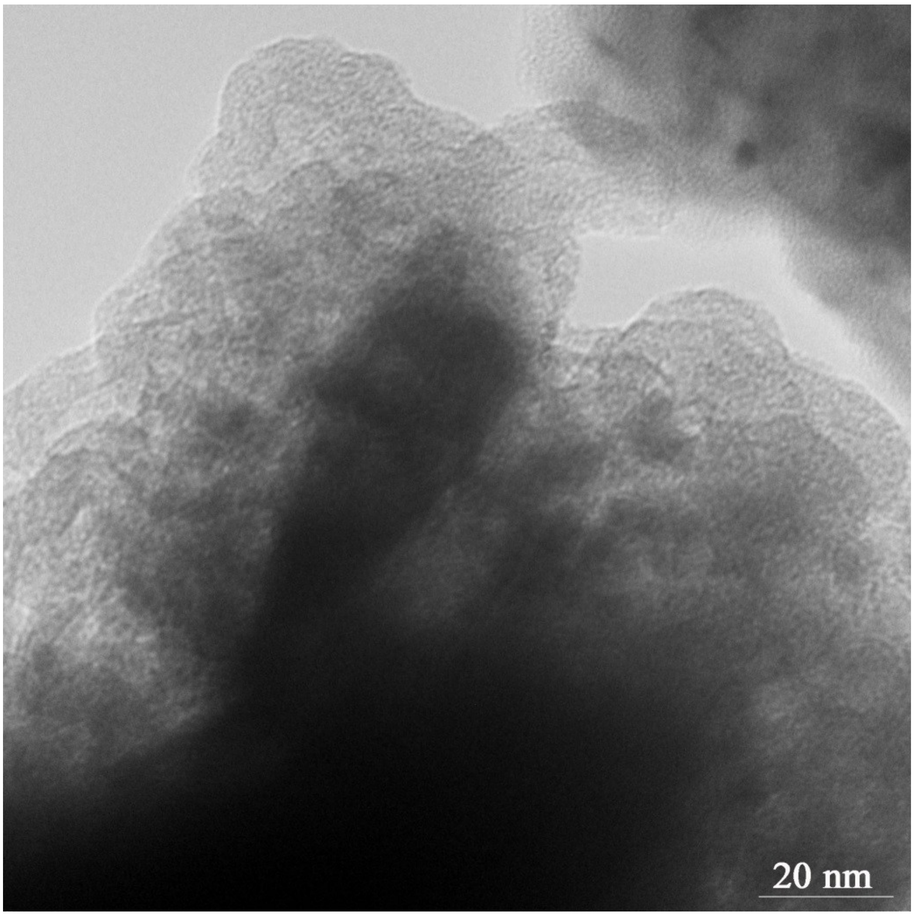

Figure S11. Representative TEM image of $FeCoCuO_x$ after OER.

Table S1. Comparison of the OER performance of different transition-metal electrocatalysts on glass carbon electrodes in 1 M KOH

Catalyst	η@ 10 mA·cm^{-2} (mV)	Tafel slope (mV·dec^{-1})	Ref.
$FeCoCuO_x$	256	42.9	This Work
IrO_2	260	45	[5]
Co-Fe-O/rGO	340	31	[6]
CoFe LDH	331	52	[7]
FeCo-ONS	308	36.8	[8]
α-$FeCoO_x$	300	33	[9]
NiFeOOH	340	60	[10]
NiFe LDH	300	40	[11]
$Ni_{0.75}Fe_{0.25}OOH$	258	-	[12]
$NiCo_{2.7}(OH)_x$	350	65	[13]
CCS Ni-Co	302	43.6	[14]
Ni-Co LDHs	350	93	[15]
NiCo LDH	367	40	[16]
$Mn_3O_4/CoSe_2$	450	49	[17]
CoMn LDH	324	43	[18]
NiFeAl	~350	158	[19]
NiCd(A)Fe	290	38	[20]

G-FeCoW	223	37	[5]

References

[1] V. Augustyn, J. Come, M.A. Lowe, J.W. Kim, P.-L. Taberna, S.H. Tolbert, H.D. Abruna, P. Simon, B. Dunn, High-rate electrochemical energy storage through Li+ intercalation pseudocapacitance, Nat. Mater., 12 (2013) 518-522.

[2] Y. Liang, Y. Li, H. Wang, J. Zhou, J. Wang, T. Regier, H. Dai, Co3O4 nanocrystals on graphene as a synergistic catalyst for oxygen reduction reaction, Nat. Mater., 10 (2011) 780-786.

[3] Y. Li, W. Zhou, H. Wang, L. Xie, Y. Liang, F. Wei, J.-C. Idrobo, S.J. Pennycook, H. Dai, An oxygen reduction electrocatalyst based on carbon nanotube-graphene complexes, Nat. Nanotechnol., 7 (2012) 394-400.

[4] M.B. Stevens, L.J. Enman, A.S. Batchellor, M.R. Cosby, A.E. Vise, C.D.M. Trang, S.W. Boettcher, Measurement Techniques for the Study of Thin Film Heterogeneous Water Oxidation Electrocatalysts, Chem. Mater., 29 (2017) 120-140.

[5] B. Zhang, X.L. Zheng, O. Voznyy, R. Comin, M. Bajdich, M. Garcia-Melchor, L.L. Han, J.X. Xu, M. Liu, L.R. Zheng, F.P.G. de Arquer, C.T. Dinh, F.J. Fan, M.J. Yuan, E. Yassitepe, N. Chen, T. Regier, P.F. Liu, Y.H. Li, P. De Luna, A. Janmohamed, H.L.L. Xin, H.G. Yang, A. Vojvodic, E.H. Sargent, Homogeneously dispersed multimetal oxygen-evolving catalysts, Science, 352 (2016) 333-337.

[6] J. Geng, L. Kuai, E. Kan, Q. Wang, B. Geng, Precious-Metal-Free Co-Fe-O/rGO Synergetic Electrocatalysts for Oxygen Evolution Reaction by a Facile Hydrothermal Route, ChemSusChem, 8 (2015) 659-664.

[7] R. Liu, Y. Wang, D. Liu, Y. Zou, S. Wang, Water-Plasma-Enabled Exfoliation of Ultrathin Layered Double Hydroxide Nanosheets with Multivacancies for Water Oxidation, Adv. Mater., 29 (2017) 1701546.

[8] L. Zhuang, L. Ge, Y. Yang, M. Li, Y. Jia, X. Yao, Z. Zhu, Ultrathin Iron-Cobalt Oxide Nanosheets with Abundant Oxygen Vacancies for the Oxygen Evolution Reaction, Adv. Mater., 29 (2017) 1606793.

[9] M.S. Burke, M.G. Kast, L. Trotochaud, A.M. Smith, S.W. Boettcher, Cobalt-Iron (Oxy)hydroxide Oxygen Evolution Electrocatalysts: The Role of Structure and Composition on Activity, Stability, and Mechanism, J. Am. Chem. Soc., 137 (2015) 3638-3648.

[10] J.R. Swierk, S. Klaus, L. Trotochaud, A.T. Bell, T.D. Tilley, Electrochemical Study of the Energetics of the Oxygen Evolution Reaction at Nickel Iron (Oxy)Hydroxide Catalysts, J. Phys. Chem. C, 119 (2015) 19022-19029.

[11] D. Friebel, M.W. Louie, M. Bajdich, K.E. Sanwald, Y. Cai, A.M. Wise, M.J. Cheng, D. Sokaras, T.C. Weng, R. Alonso-Mori, R.C. Davis, J.R. Bargar, J.K. Norskov, A. Nilsson, A.T. Bell, Identification of Highly Active Fe Sites in (Ni,Fe)OOH for Electrocatalytic Water Splitting, J. Am. Chem. Soc., 137 (2015) 1305-1313.

[12] A.S. Batchellor, S.W. Boettcher, Pulse-Electrodeposited Ni-Fe (Oxy)hydroxide Oxygen Evolution Electrocatalysts with High Geometric and Intrinsic Activities at Large Mass Loadings, ACS Catal., 5 (2015) 6680-6689.

[13] J. Nai, H. Yin, T. You, L. Zheng, J. Zhang, P. Wang, Z. Jin, Y. Tian, J. Liu, Z. Tang, L. Guo, Efficient Electrocatalytic Water Oxidation by Using Amorphous Ni-Co Double Hydroxides Nanocages, Adv. Energy Mater., 5 (2015) 1401880.

[14] S.-H. Bae, J.-E. Kim, H. Randriamahazaka, S.-Y. Moon, J.-Y. Park, I.-K. Oh, Seamlessly

Conductive 3D Nanoarchitecture of Core-Shell Ni-Co Nanowire Network for Highly Efficient Oxygen Evolution, Adv. Energy Mater., 7 (2017) 1601492.

[15] C. Wang, J. Zhang, C. Shi, D. Cai, Facile Synthesis of Ni-Co LDH Nanocages with Improved Electrocatalytic Activity for Water Oxidation Reaction, Int. J. Electrochem. Sci., 12 (2017) 10003-10014.

[16] H. Liang, F. Meng, M. Caban-Acevedo, L. Li, A. Forticaux, L. Xiu, Z. Wang, S. Jin, Hydrothermal Continuous Flow Synthesis and Exfoliation of NiCo Layered Double Hydroxide Nanosheets for Enhanced Oxygen Evolution Catalysis, Nano Lett., 15 (2015) 1421-1427.

[17] M.-R. Gao, Y.-F. Xu, J. Jiang, Y.-R. Zheng, S.-H. Yu, Water Oxidation Electrocatalyzed by an Efficient Mn3O4/CoSe2 Nanocomposite, J. Am. Chem. Soc., 134 (2012) 2930-2933.

[18] F. Song, X. Hu, Ultrathin Cobalt-Manganese Layered Double Hydroxide Is an Efficient Oxygen Evolution Catalyst, J. Am. Chem. Soc., 136 (2014) 16481-16484.

[19] X. Cui, B. Zhang, C. Zeng, H. Wen, S. Guo, Monolithic nanoporous Ni-Fe alloy by dealloying laser processed Ni-Fe-Al as electrocatalyst toward oxygen evolution reaction, Int. J. Hydrogen Energy, 43 (2018) 15234-15244.

[20] J.-H. Kim, D.H. Youn, K. Kawashima, J. Lin, H. Lim, C.B. Mullins, An active nanoporous Ni(Fe) OER electrocatalyst via selective dissolution of Cd in alkaline media, Appl. Catal. B: Environ., 225 (2018) 1-7.